ORIGINAL PAPER

Landslide susceptibility mapping and rock slope stability assessment using frequency ratio and kinematic analysis in the mountains of Mgulat area, Northern Ethiopia

Gebremedhin Berhane[1] · Mulubrhan Kebede[2] · Nawal Alfarrah[3]

Abstract

Landslides, mainly triggered by rainfall, are one of the most common natural hazards in the northern and central highlands of Ethiopia, resulting in the loss of human life and property. As part of the Ethiopian highlands, Mgulat Mountain (88.6 km^2) is a typical example for the occurrence of landslides and associated damages. The main aim of this research was to generate landslide susceptibility map (LSM) for the first time by considering various causative factors typical for the Mgulat Mountain area. The methods used include frequency ratio (FR) and kinematic analysis (KA) supported by GIS tools. The research involved conventional fieldwork (e.g., geological mapping, landslides inventory) and analysis and interpretation of images. From the geological mapping, major rock units were identified: quaternary deposit, basalt, red sandstone, tillite, and white sandstone. A total of 220 landslides (15.45 km^2) were identified in the study area from field survey, Google Earth and aerial photo interpretation. Five causative factors (lithology, slope steepness, distance from drainage, land use-land cover (LULC), and slope aspect) were selected based on their contribution to landslide initiation as the landslide conditioning factors for generation of the LSM. From the five causative factors, lithology and slope steepness were found to be influential as landslide conditioning factors. Specifically, lithology (red sandstone and tillite), distance to stream (0 to 300 m), LULC (bare land and settlement), and slope steepness (> 25°) have FR > 1, indicating a high relationship with landslide occurrence. Based on the generated LSM, five susceptibility classes or zones were identified (very low, low, moderate, high, and very high susceptibility). The area of each class as percentage of total area was found to be 19.53, 24.15, 22.57, 18.74, and 15.01%, for the very low to the very high class, respectively. The results of KA show potentially and marginally planar, topple, and wedge failures. The generated LSM can serve as an important tool or guide for further land-use planning and to prevent and mitigate landslide-related risks. Consequently, to consider cost-effective and technically sound mitigation measures, detailed and site-specific multidisciplinary investigations are recommended.

Keywords Causative factors · Geology · GIS · Inventory mapping · Slope stability · Validation

✉ Gebremedhin Berhane
gmedhin_berhane@yahoo.com

Mulubrhan Kebede
mulubrhankebede21@gmail.com

Nawal Alfarrah
Nawalalfarrah@gmail.com

[1] School of Earth Sciences, Mekelle University, P.O. Box 1202, Mekelle, Ethiopia

[2] Aksum University, Aksum, Ethiopia

[3] Ghent University, Ghent, Belgium

Introduction

Landslides are among the most common geohazard in many parts of the world (Haque et al. 2019; Saadatkhah et al. 2014). They claims and damages human life and infrastructures in many mountainous regions (Corominas et al. 2014; Kanungo et al. 2009; Mohan et al. 2011; Yalcin et al. 2011; Wyllie 2015). The impacts of these events on the local and global economy are huge (Yalcin et al. 2011; AGU 2017), and mountains remain to be the top agenda in terms of geohazard (Debarbieux and Rudaz 2015; United Nations 2016; Price et al. 2019). Many authors and researchers defined landslide as any down slope movement of earth materials due to gravity (Cruden 1991; Highland and Bobrowsky 2008; Hungr et al. 2013; Varnes 1984). They are responsible for the damages of

hundreds of billions of properties, transportation networks, buildings and other structures, deaths, and injuries every year. Therefore, identification and mapping of landslide-prone mountain areas is considered important to guarantee the safety of human life and property and to support land planners and decision makers (Zhou et al. 2018).

In Ethiopia, landslide-generated damages are serious problems to the planners and decision makers at various levels of the government (Woldearegay 2013) that cause many social, economical, and geomorphological impacts (Broothaerts et al. 2012). According to Abebe et al. (2010), the most common triggering factor for landslide incidence in Ethiopia is heavy rainfall. Ayenew and Barbieri (2005) also pointed out that gully erosion is one of the triggering factors responsible for generating landslides due to erodible materials and heavy floods. In most rock masses, the large and closely spaced joints are the main causes for rock falls and toppling. In many mountainous areas, rock discontinuities are one of the causative factors for various types of landslides and mass movements (Ayenew and Barbieri 2005; Sun et al. 2018). Most regions of the northern Ethiopia are rugged with steep hillside slopes, steep river banks, and steep road cut slopes that have long histories of landslide activity (Ayenew and Barbieri 2005).

Landslide susceptibility analyses are the initial step in understanding and minimizing landslide damages. Such analysis can be implemented using various methods such as statistical (e.g., frequency ratio (FR)), heuristic (e.g., analytical hierarchy process (AHP)) methods (Corominas et al. 2014; Hong et al. 2016; Nicu 2018; Sun et al. 2018; Pourghasemi et al. 2018; Yalcin et al. 2011), and kinematic analysis (KA). As explained by Broothaerts et al. (2012), landslides are the result of a combination of both intrinsic and triggering factors. A landslide inventory map shows the areal distribution of current and past landslide areas and their characteristics. Analysis and summation of weighted values of landslide conditioning factors such as aspect, elevation, distance to fault, distance to stream, etc. are the basic factors for landslide susceptibility map (LSM) preparation (Demir et al. 2013; Hong et al. 2016; Sun et al. 2018). Analysis of rock slope stability using KA indicates the role of discontinuities for development of landslides (Baharuddin et al. 2016).

To mitigate landslide damage, it is necessary to evaluate and analyze the causative factors, hazard, vulnerability, and risk along with identification and delineation of landslide-susceptible areas (Hong et al. 2016; Pourghasemi and Rahmatib 2018; Saadatkhah et al. 2014). This LSM was carried out once all field evidence-related data and laboratory test results are collected and analyzed. Basically, a LSM subdivides or classifies a given terrain or area into zones with differing likelihoods that landslides or geomorphological processes of different types may occur (Corominas et al. 2014). It predicts "where" landslides are likely to occur (Guzzetti et al. 2005; Reichenbach et al. 2018). Landslide susceptibility

assessment is considered an initial step toward a landslide hazard and risk assessment, but according to Corominas et al. (2014), it can also be an end product in itself that can be used in land-use planning and environmental impact assessment. This is especially the case in situations where insufficient information is available on past landslide occurrence to allow the spatial and temporal probabilities of events to be assessed. As landslide susceptibility maps primarily provide a proposed ranking of terrain units in terms of spatial probability of occurrence, they do not explicitly convey information on landslide return periods.

The Mgulat Mountain area is a typical example for its data scarcity. LSMs contain information on the type of landslides that might occur and on their spatial likelihood of occurrence in terms of identifying the most probable initiation areas (based on a combination of geological, geomorphological, and LULC conditions).

The main objective of this study was to describe the landslide causative factors and produce LSM using FR and to assess stability of selected rock slopes using KA method. Landslide susceptibility map is the division of land surface into well-defined zones and ranking the zones based on the degree of potential landslide susceptibility. It is used to identify places of landslide occurrences on the basis of a set of causative factors (Hong et al. 2016; Kanungo et al. 2009) in which the value represents the relative susceptibility to future landslide occurrence, as higher values are associated with high landslide susceptibility (Avinash and Ashamanjari 2010).

Description of the study area

Mgulat area is located in the northern part of Ethiopia, Tigray Regional State, Eastern Zone within Ganta-Afeshum Woreda (district). Geographically, it is bounded between 1,570,000 to 1,582,000 mN latitude and 530,000 to 546,000 mE longitude (UTM Zone 37N). The study area covers 88.6 km^2, and it is characterized by a dendritic drainage pattern (Fig. 1). The elevation ranges from 2050 to 3250 m a.s.l. The mean monthly rainfall of the area ranges from 4.4 mm in February to 229.7 mm in July with a total annual mean rainfall of 707.6 mm. Nearly 66% of the annual rainfall occurs only in the months of June, July, and August. According to field observation and data from local people, many of the past landslides occurred during these months. The minimum and maximum mean annual temperature of Mgulat area is 10.7 and 22.8 °C, respectively.

The present study is located in both rugged and steep topographic terrain with little road cuttings. As a result, active landslides are common and occur every year in the study area, resulting in damages to settlements and farmlands.
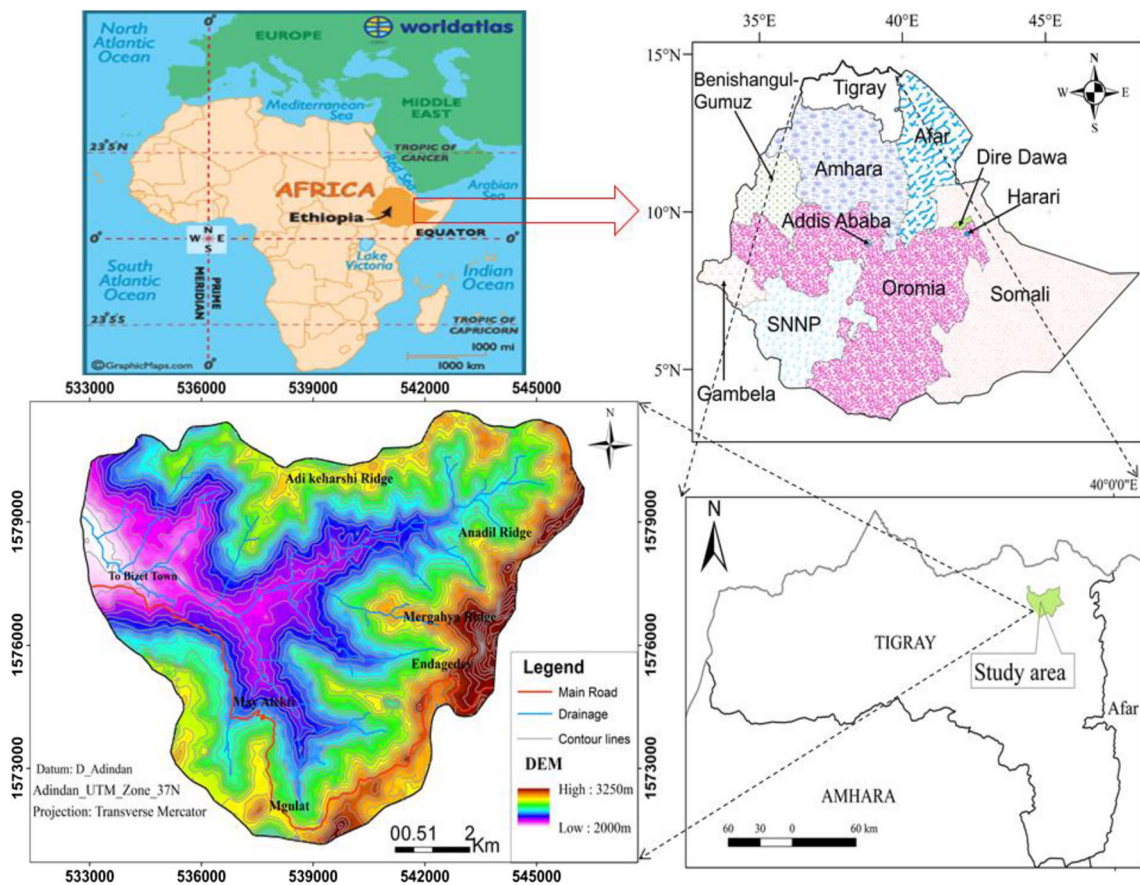
Fig. 1 Location map of Mgulat area (with 40 m contour interval and DEM) and its surroundings with reference to Ethiopia and Tigray Regional State

Statement of the problem

Landslide triggered by rainfall is one of the common geohazards in the highlands of Ethiopia, especially in northern and central Ethiopian highlands, mainly responsible for the losses of human life and property. As part of the Ethiopian highlands, in Mgulat area (Fig. 1), a number of damages were reported due to landslides. A recent example is the 24th August 2018 landslide event, which killed six people and destroyed farmland, settlement, and property (Fig. 2a). In addition, a rock fall event in August 2017 claimed the life of one woman near Mgulat village (Fig. 2b). The problem is wide

Fig. 2 Field photographs of **a** the 24th August 2018 landslide and **b** a rock fall event in August 2017. Photographs were taken by the second author in September, 2018

and significant. Emanating from these problems, the aim of this research was to assess and understand the causes and failure mechanisms, carry out the mapping of the active and past landslides, and, finally, generate LSM. The ultimate goal was to improve the current spatial land-use plan and guide and support local and regional administrative bodies in managing landslide risk.

Methods and materials

For the accomplishment of this research, the FR method and KA approach were selected considering the reliability and availability of data. Generally, the following main steps or approaches were adopted during the research work:

1. Data collection (Wieczorek 1984; Crozier 2005) and construction of spatial database from which the relevant causative factors were extracted and selected,
2. Assessment and generation of LSM using the relationship between the inventoried landslides and selected site-specific causative factors, and
3. Verification and validation of the generated LSM using the inventoried landslides and other approaches.

The slope steepness, slope aspect, drainage, and elevation maps of the study site were extracted from digital elevation model (DEM) with 30 m resolution generated from NASA's Shuttle Radar Topography Mission (SRTM) in 2000 (http://dds.cr.USGS.gov/SRTM/version2_1/SRTM3/ Africa/).

Topographic maps Adigrat (1439 C2), and Nebelet (1439 C4) sheets with a scale of 1:50,000) (EMA 1997) were used as a base map for field data collections. Regional geological map of Adigrat (ND 37-7) (Garland 1980) with a scale of 1: 250,000 and fieldwork campaign were used for the compilation and preparation of the geological map of Mgulat area.

The following calculations (equations below) were used to generate the thematic maps and LSM using FR and the spatial analyst tool of ArcGIS (ESRI 2010). Figure 3 shows the simplified overall methods and approaches.

$$\text{Area} \left(\text{km}^2 \right) = \frac{\text{Number of pixel} \times 900 \text{ m}^2}{1,000,000} \qquad (1)$$

where 900 m^2 = 30 m × 30 m pixel (from DEM) and 1,000,000 = 1000 × 1000, since the 30 m × 30 m is in meter and when it is converted to km^2, 1000 m × 1000 m = 1,000,000 m^2.

FR is the ratio of occurrence probability to non-occurrence probability for a specific attribute. Several researchers used FR for landslide susceptibility mapping (e.g., Akgun et al. 2008; Donati and Turrini 2002; Lee and Choi 2003; Lee et al. 2002; Luzi et al. 2000; Lee and Talib 2005; Pradhan and Lee 2009; Sun et al. 2018; Vijith and Madhu 2007; Zezere et al. 2004; Zhou et al. 2018). The FR value for each landside conditioning sub-class was determined using Eq. (2). The novelty of this article relies on the use and testing of FR for the first time for Mgulat mountainous area with no existing landslide inventory database.

$$\text{FR} = \frac{(\text{Number of landslide pixels in a sub-class/Total number of landslide pixels})}{(\text{Total number of pixels in a sub-class/Total number of pixels in the study area})} \qquad (2)$$

The landslide susceptibility index (LSI) was calculated during the overlay by adding all the FR values of each factor using Eq. (3). The LSI represents the relative susceptibility to landslide occurrence (the greater the value, the higher the susceptibility to landslide occurrence and vice versa) (Chalkias et al. 2014).

$$\text{LSI} \left(\% \right) = \text{FR} \left(\text{Lithology} \right) + \text{FR} \left(\text{Slope} \right) + \text{FR} \left(\text{Distance from stream} \right) + \text{FR} \left(\text{LULC} \right) + \text{FR} \left(\text{Slope aspect} \right) \qquad (3)$$

Geological context

According to Mengesha et al. (1996), the lithological units of Ethiopia fall into three major categories: Precambrian basement, Late Paleozoic to Paleogene sediments, and Cenozoic volcanic and associated sedimentary rocks. The stratigraphic succession of Northern Ethiopia is divided

into Precambrian basement (Tsalet group), Enticho sandstones (white sandstone), Edaga Arbi Glacial (tillite), Adigrat sandstones (red sandstone), Antalo limestone, Agula shale, Amba Aradam Formation, Trap series, Mekelle dolerites, and Axum-Adwa plugs (Sembroni et al. 2017). The local geology of the study area was mapped through field investigation (Fig. 4).
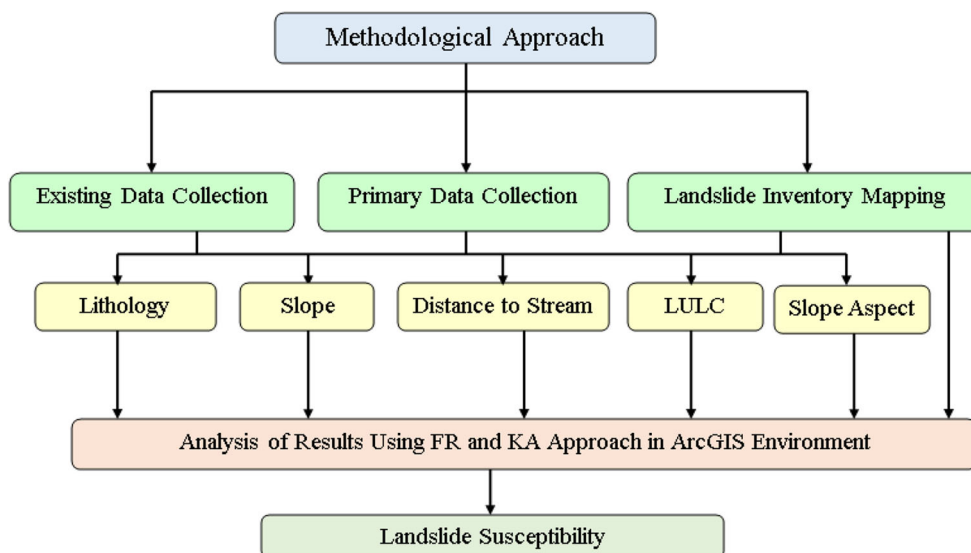
The area consists of five lithological units (Figs. 4 and 5): Quaternary deposits (residual soil and alluvial deposits) (Fig. 5b), basalt (aphanatic, amygdaloidal, agglomeratic, and columnar basalt varieties) (Fig. 5a, c), red sandstone, tillite, and white sandstone. A larger proportion of the study area is covered by basalt (Fig. 4). The tillite unit is weak and impervious, underlain by white sandstone and overlain by red sandstone. The presence of open discontinuities in the red sandstone results in direct percolation of rain water responsible for development of pore water pressure and finally for the failure
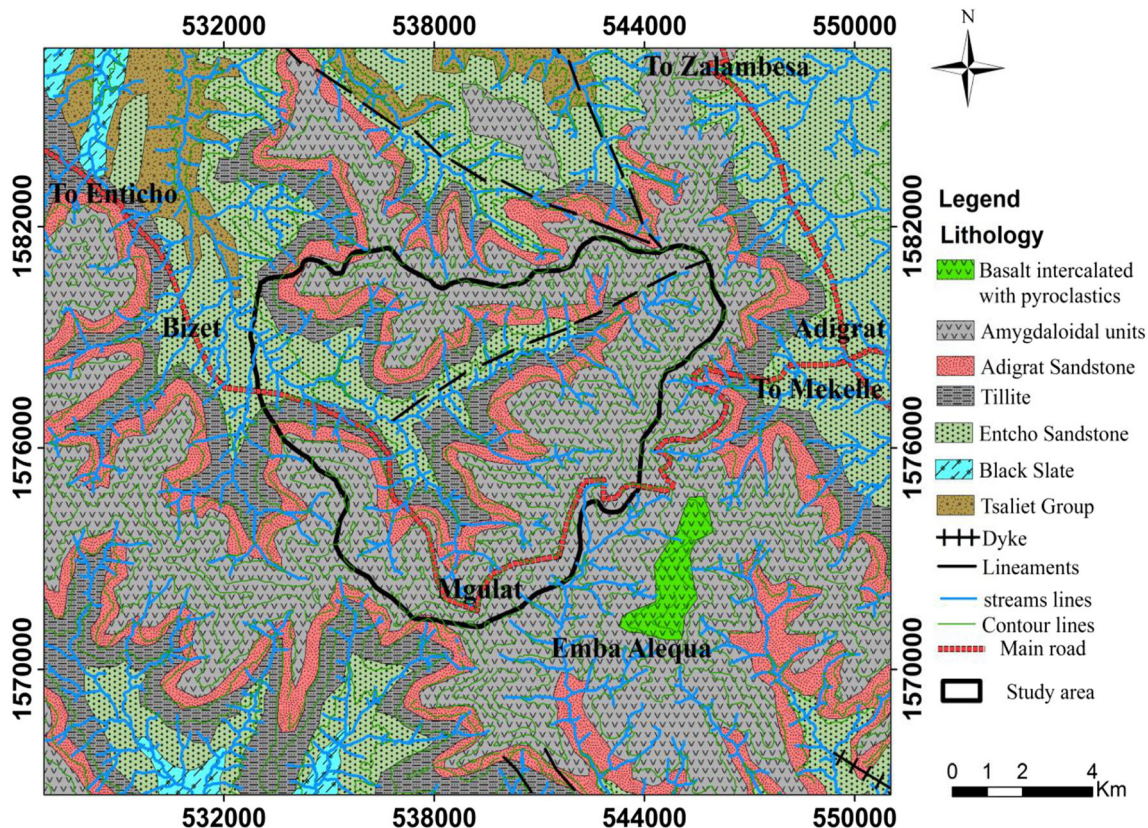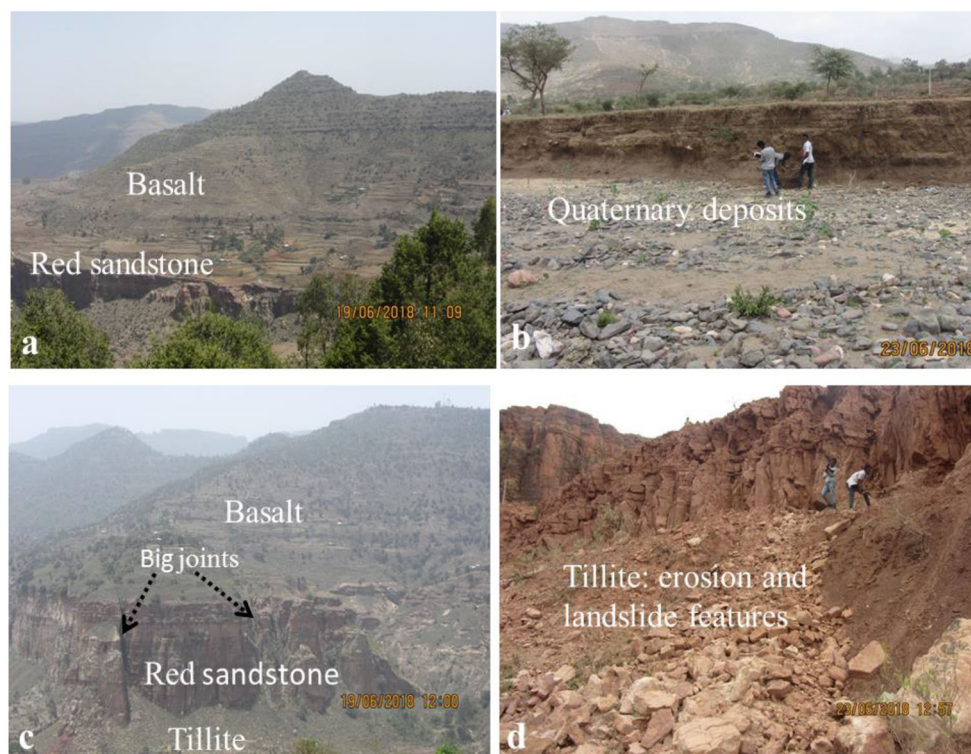

Fig. 4 Regional geological map of Mgulat area and its surrounding showing the coverage of Mesozoic and Cenozoic sedimentary and volcanic rocks (modified from Garland 1980). The study area boundary is indicated in the center of the map with bold line. Datum: Adindan UTM Zone 37N and projection: transverse Mercator

of slopes in the form of rock fall and topple. The erodibility nature of the tillite unit also contributes to the occurrence of numerous landslides (e.g., debris flow, rock fall, topples, etc.) in the tillite itself (Fig. 5d) and red sandstone unit (Fig. 5a, c).

Results and discussion

### Thematic data layers and landslide inventory mapping

The study began with the preparation of a landslide inventory map based on extensive field work and Google Earth image interpretation (Wieczorek 1984; Crozier 2005). Inventory mapping was used to show and locate the type and characteristics of landslides and related features that occurred in the past. The landslide inventory mapping of the present study was used as a basis for the LSM. Landslide inventory map is very necessary for understanding the relationship between the landslide events and the possible controlling parameters of landslides (Ercanoglu and Gokceoglu 2004). A total of 220 landslides were inventoried and, out of these, 205 landslides were used for analysis, while 15 of them were excluded randomly from the analysis for the validation of the LSM. From the total 220 landslides, some of them are giant blocks that affect large areas, while the others cover very small areas. From rasterized area calculation of the landslides, 0.366 km^2 is the largest landslide whereas 155 m^2 is the smallest one (Fig. 6). The landslides are

grouped into four types based on Varnes (1978) classification system, (a) 92 (41.8%) rock fall, (b) 57 (25.9%) complex, (c) 40 (18.2%) topples, and (d) 31 (14.1%) debris flow.

Causative factors and landslide occurrence

To produce LSM and minimize losses incurred by landslide events, it is indispensable to create a good understanding of the causative factors. In the present study, numerous causative factors play an important role simultaneously and in a complex manner. The right choice or selection of causative factors depends on the modes and type of landslides, conditions and nature of the study site, extent and scope of the analysis, availability of data set, and analysis methods selected (Tseng et al. 2015). Generally, there is no agreement on the universal guidelines for selecting landslide conditioning factors (Pradhan and Lee 2010) applicable everywhere. In the present study, five causative factors were selected, among eight pre-selected factors, for generating LSM based on their contribution toward landslide initiation and field verification and are among the most commonly used in the literature to assess landslide susceptibility (Pradhan and Lee 2010; Pourghasemi et al. 2013). The main causative factors are lithology, slope steepness, distance to stream, LULC, and slope aspect (Figs. 7, 8a, b, and 9a, b). Distance to road, elevation, and distance to fault were excluded from the analysis due to their weak relationship with landslide occurrence, which was verified by field observation and landslide inventory map. In addition, along most of the

Fig. 6 Landslide inventory map of Mgulat area. Dendritic drainage system with overall flow toward the northwest direction is shown. Datum: Adindan UTM Zone 37N and projection: transverse Mercator
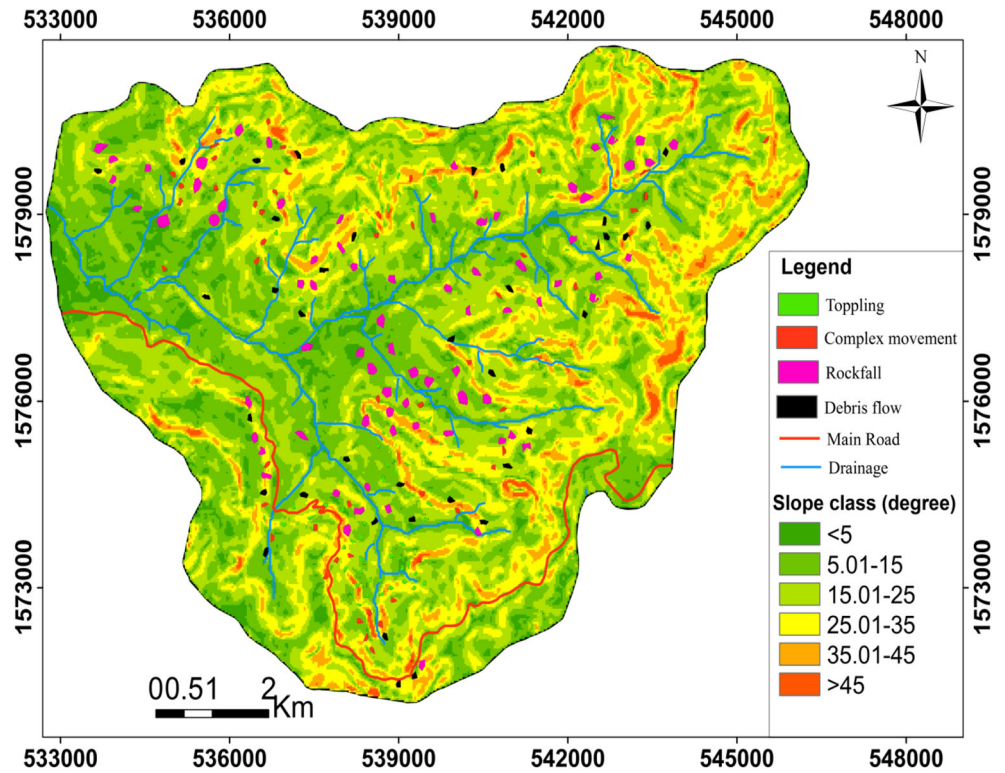

main road sides, an engineering solution was already provided, which is a retaining wall made of masonry. Hence, it cannot be a major cause for future landslide occurrences. The relationship between causative factors and landslide occurrence was evaluated based on their FR values.

Rainfall and manmade activities are the main extrinsic variables or temporary factors contributing to landslide occurrence in the area. Manmade activities include road cut, construction materials extraction or excavation and deforestation, but their relationship with landslide occurrence was found to be

Fig. 7 Lithological map of Mgulat area. Lithology is considered as a landslide conditioning factor. Slight variations with Fig. 4 are attributed to the scale and presence of localized lithological units not included in Fig. 4. Kinematic rock slope stability analysis was conducted at three locations (R1, R2, and R3). Datum: Adindan UTM Zone 37N and projection: transverse Mercator
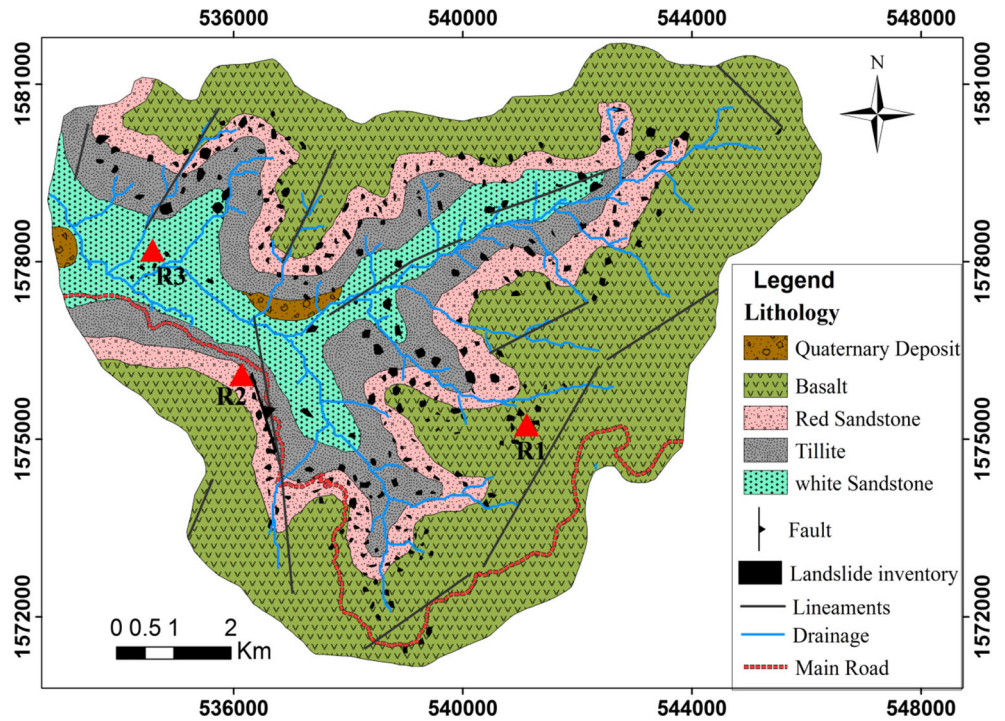
Fig. 8 Conditioning factors maps. **a** Slope aspect (degree) (top) and **b** distance to stream (m) (bottom). Datum: Adindan UTM Zone 37N and projection: transverse Mercator
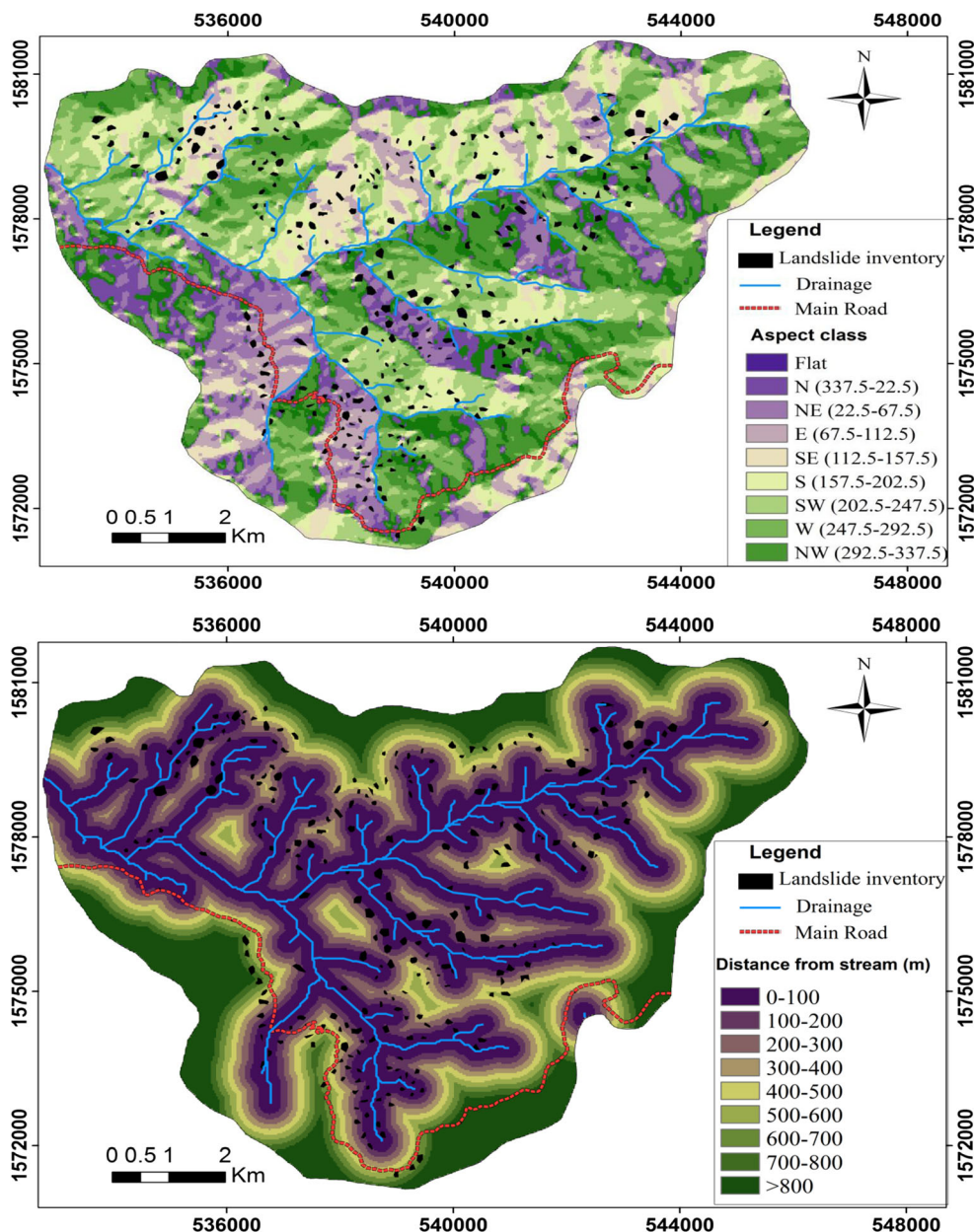

insignificant. Most of the roads' cut sides are stabilized with masonry retaining structures. The predominant causes for landslide occurrence in the study area are lithology and slope steepness (causative factors) and rainfall (triggering factor). The selection of these factors depends mainly on the availability of data for the study area and their significance or contribution to landslide occurrences (Figs. 7, 8a, b, and 9a, b).

All the selected causative factors (lithology, slope steepness, distance to stream, LULC, and slope aspect) were analyzed to generate LSM using the FR method. For each factor, the FR value of each class was determined to understand the most influencing factors as described in Table 1. Accordingly, factors with FR > 1 have strong relationship, whereas those with FR < 1 have weak relationship with landslide occurrence.

For each of the thematic maps, the FR value for each class was assigned using the ArcGIS spatial analyst tool (Fig. 10). The LSI values of the present study were classified into very low, low, moderate, high, and very high susceptibility classes based on the degree of susceptibility by using the natural breaks provided in ArcGIS. The areal percentage of landslides (Table 2) for very low, low, and moderate susceptibility classes are 1.32, 8.35, and 20.39%, respectively, while percentage distribution for the high and very high classes are higher (24.5 and 45.44%, respectively). Hence, it can be fairly inferred that the landslide susceptibility zones reflect the existing or observed field instability conditions as a function of the landslide inventory map.

Fig. 9 Conditioning factors maps. **a** LULC (top) and **b** slope class (degree) (bottom). Datum: Adindan UTM Zone 37N and projection: transverse Mercator
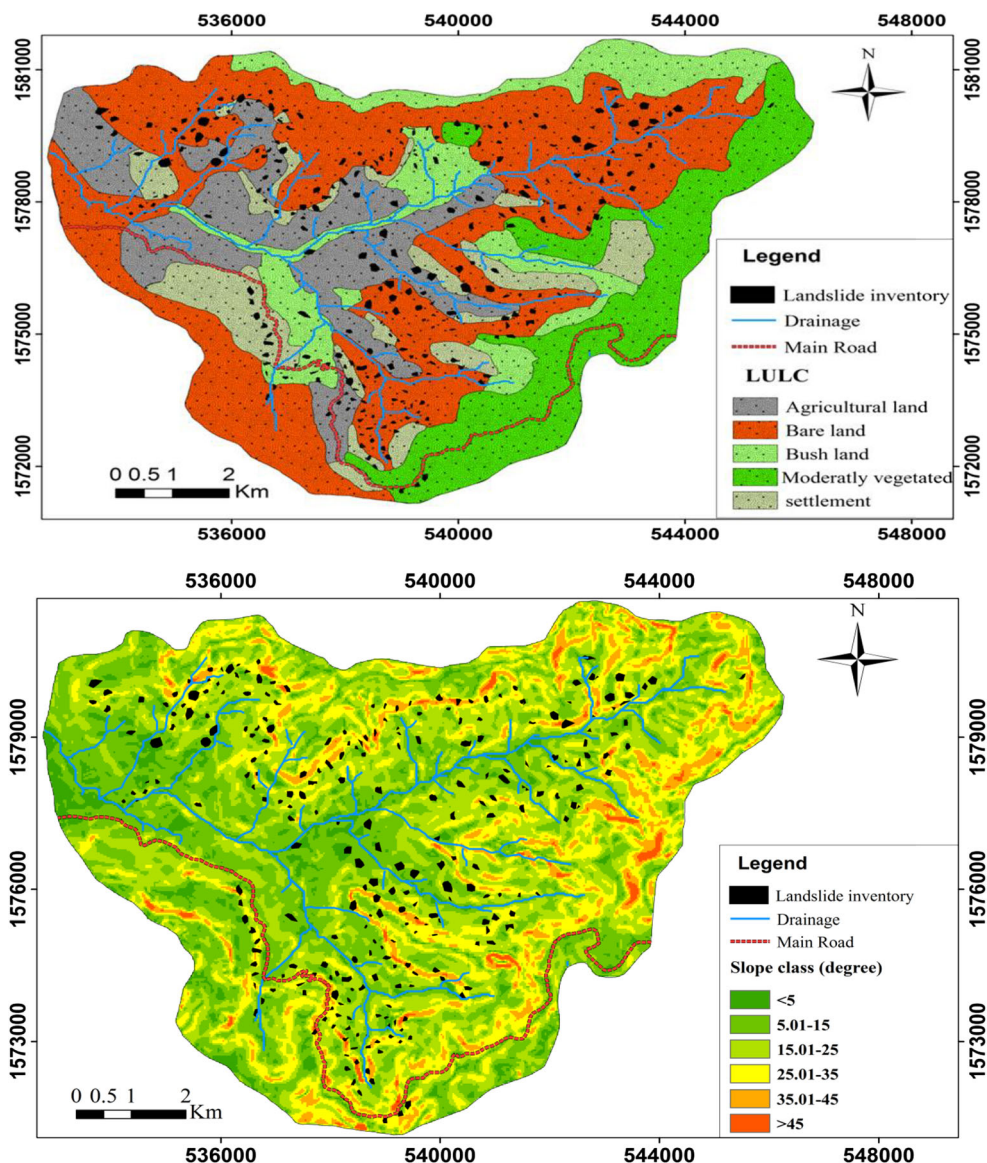
A schematic representation of the mechanisms of the landslides, particularly rock falls and topples, for the study area is depicted in Fig. 11. The schematic representation shows rainfall infiltration through vertical joints and interconnected pores. The infiltrated water produces pore water pressure due to the presence of impervious units below (tillite) and resulted in the occurrence of a variety of landslides (e.g., rock fall, topples). The vertical joints in the red sandstone were developed due to stress relief toward the cliffs.

Verification and validation of the LSM

Validation is an essential component in landslide susceptibility mapping to confirm the efficiency, applicability and scientific significance of the methods used (Frattini et al. 2010;

Zhou et al. 2018). To verify and validate the generated LSM, four approaches were used as depicted below.

Landslide density or frequency

The LSM obtained from FR was verified through a comparison of the past landslide distribution and the generated LSM, which is sometimes called the accuracy statistic method (Zhou et al. 2018) or landside density or frequency (Khan et al. 2019; Reichenbach et al. 2018). In this approach, the landslide distribution in different susceptibility class was statistically analyzed. From the landslide distribution, 45.5% of the inventoried landslide areas (14.35 km^2) fall in the very high susceptibility class, 24.5% fall in the high, 20.4% fall in the moderate, 8.4% fall in the low, and 1.32% fall in the very low susceptibility class. From this verification or comparison of

Table 1 FR values of the landslide conditioning or causative parameters (factors)

Factors (thematic layers)	Classes	% of total area (a)	% of landslide area (b)	FR (b/a)
Lithology	White sandstone	11.97	3.64	0.30
	Tillite	19.28	21.20	*1.10*
	Red sandstone	16.35	45.66	*2.79*
	Basalt	51.42	28.8	0.56
	Quaternary deposit	0.98	0.70	0.71
Slope (deg)	< 5	5.85	2.66	0.45
	5.01–15	33.18	22.13	0.67
	15.01–25	35.04	35.98	*1.03*
	25.01–35	18.66	27.56	*1.48*
	35.01–45	6.19	8.79	*1.42*
	> 45	1.08	2.88	*2.67*
Distance from drainage (m)	0–100	11.24	38.05	*3.39*
	100–200	10.48	19.9	*1.90*
	200–300	10.08	15.39	*1.53*
	300–400	9.43	9.30	0.99
	400–500	9.12	7.47	0.82
	500–600	8.82	7.37	0.84
	600–700	8.35	2.26	0.27
	700–800	7.43	0.10	0.01
	> 800	25.09	0.00	0.00
Aspect (deg)	Flat	0.00	0.0042	0.00
	N (337.5–22.5)	15.47	18.72	*1.21*
	NE (22.5–67.5)	10.27	11.43	*1.11*
	E (67.5–112.5)	7.48	9.72	*1.30*
	SE (112.5–157.5)	8.95	14.59	*1.63*
	S (157.5–202.5)	11.48	16.45	*1.43*
	SW (202.5–247.5)	15.88	11.27	0.71
	W (247.5–292.5)	14.30	11.01	0.77
	NW (292.5–337.5)	16.16	7.11	0.44
LULC	Agricultural land	17.09	12.80	0.75
	Bush land	14.04	5.68	0.40
	Bare land	41.56	63.16	*1.52*
	Settlement	10.22	13.57	*1.33*
	Moderately vegetated	17.09	4.79	0.28

Values greater than one (in italics) have positive relation with landslide

the LSM with inventoried landslides, 70% of the existing landslide areas fall in the high and very high susceptible classes, indicating good performance of FR model (Fig. 12). This shows a gradual increase in percentage distribution of landslide occurrences (in terms of area) from very low susceptible class to very high susceptible class. This result was found to be similar and in agreement with different researchers elsewhere (e.g., Frattini et al. 2010; Sarkar and Kanungo 2004; Yalcin et al. 2011; Yan et al. 2018; Zhou et al. 2018). Moreover, 43.68% of the whole study area is marked as belonging to the high or very high susceptibility classes. Field observations confirmed that areas of high susceptible zones showed significant indications of slope instabilities marked by

old landslides, intensive erosion, and steep cliffs with presence of discontinuities liable for future landslide events.

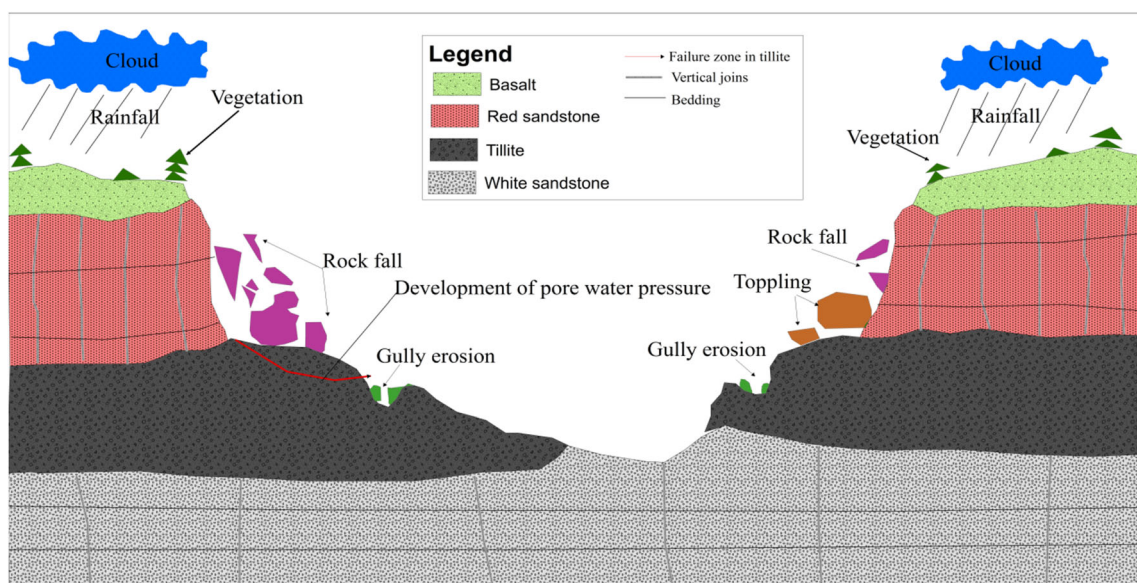## Validation using a landslide subset

As an independent verification approach, 15 inventoried landslides randomly selected were excluded from the FR analysis for verification purposes (validating data sets). The 15 inventoried landslides were superimposed over the generated LSM to check its landslide predictability power. The result show that 86.6% (13 of the 15 landslides) fall in the very high and high susceptibility classes and 13.3% (2 of the 15 landslides) fall in the moderate susceptibility zone, whereas none

Fig. 10 Generated landslide susceptibility map of Mgulat area. Datum: Adindan UTM Zone 37N and projection: transverse Mercator
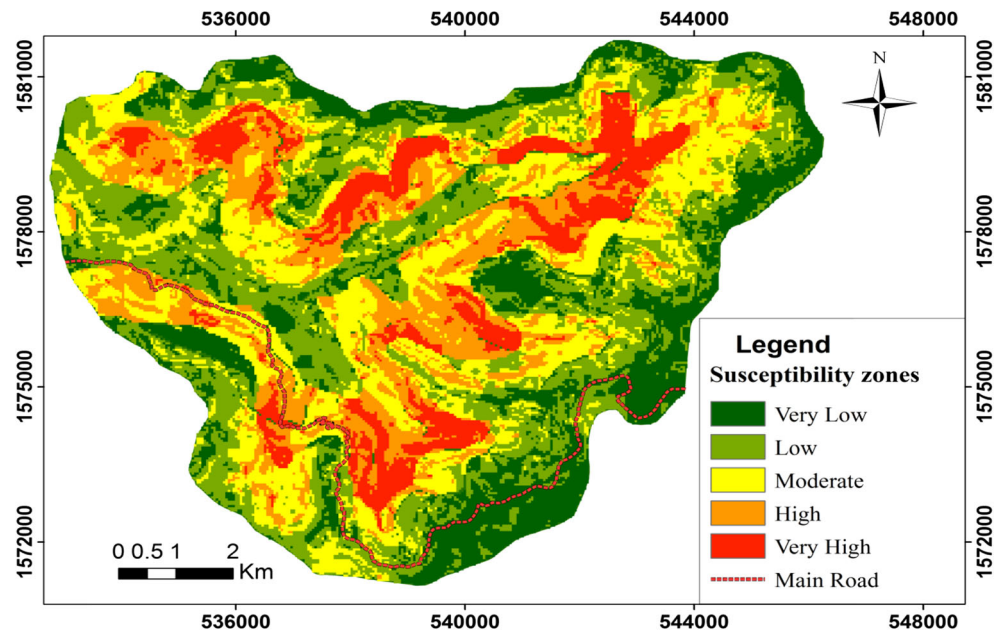

Table 2 Statistical summary of the inventoried landslides in the Mgulat Mountain

Landslide susceptibility levels	Area (km^2) of total study area	% distribution of the total study area	Area (km^2) of past landslides	% distribution of the past landslides
Very high	17.3	19.53	6.53	45.44
High	21.4	24.15	3.52	24.50
Moderate	20.0	22.57	2.93	20.39
Low	16.6	18.74	1.20	8.35
Very low	13.3	15.01	0.19	1.32

Fig. 11 Conceptual model showing rock fall and topple occurrence and mechanisms (not to scale, approximately in E-W direction)

Fig. 12 Statistical summary of LSM zones with percentage distribution of past landslides occurrence and total study area
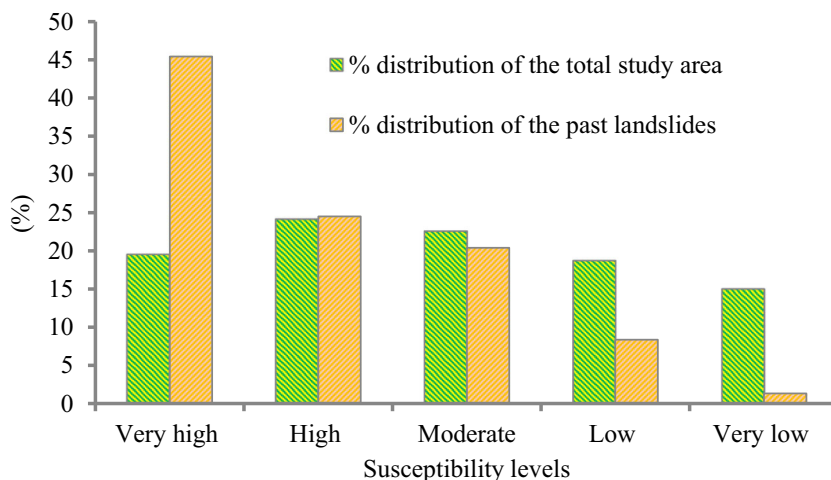
of the landslides fall in the very low and low susceptibility classes (Table 3, Fig. 13). This is a good sign of the reliability and predictability power of the generated LSM.

Success rate curve

Success rate curve is shown in Fig. 14 which was used to validate the developed landslide susceptibility map (Fig. 10). The success rate curve is generated from the LSI (Khan et al. 2019; Reichenbach et al. 2018). It is a quantitative measure of the predictive performance of the statistical model. It is used to predict the total area of landslide distribution (inventoried map) by comparing the landslide susceptibility index with the cumulative landslide occurrence in terms of areal coverage. Pradhan et al. (2014) and other researchers suggest that prediction power values > 70% in the very high and high susceptibility classes are generally considered satisfactory for prediction of the ground truth. The curve of the present study predicted that 10% of the pixels with the highest LSI values account for 72% of the total landslide pixels (Fig. 14).

Kinematic rock slope stability analysis

Kinematic rock slope stability analysis is used to determine or check whether the slope is kinematically stable or not without

consideration of associated forces. The analysis helps to distinguish which discontinuities have favorable conditions that could actually lead to failure with respect to specific slope geometry. Classification and characterization (mainly the discontinuity parameters, Table 4) of rocks are input parameters for the determination of the type of failures in the rock slopes. ROCKPACK III software (Rockware 2003) was used for kinematic slope analysis. The analysis was carried out on three different lithological units (see Fig. 7 for R1, R2, and R3 locations): basalt, red sandstone, and white sandstone (Table 4). These lithologic units are the dominant in the study site. The first rock slope analysis was carried out on the basalt in the southeastern part of the study area (R1 in Fig. 7). The basalt is characterized by moderate to high degree of weathering with some discontinuities of varied orientations. From the analysis, potentially planar, potentially toppling, and marginally wedge types of failures were identified (Fig. 15).

The second rock slope analysis was performed on the red sandstone in the eastern part of the study area (R2 in Fig. 7). The red sandstone is characterized by closely-spaced and vertical master joints and moderate to high degree of weathering. From the analysis, potentially planar, potentially wedge and marginally topple and planar types of failures were identified (Fig. 16).

The third rock slope analysis was carried out on the white sandstone in the eastern part of the study area (R3 in Fig. 7).

Table 3 Areal percentage of the 15 validating landslides for the susceptibility classes

Susceptibility class	Number of landslides	Percentage of landslide distribution (%)
Very low susceptibility class	0	0.0
Low susceptibility class	0	0.0
Moderate susceptibility class	2	13.4
High susceptibility class	6	40.0
Very high susceptibility class	7	46.6

Fig. 13 Superimposed 15 validating landslide areas over the generated LSM
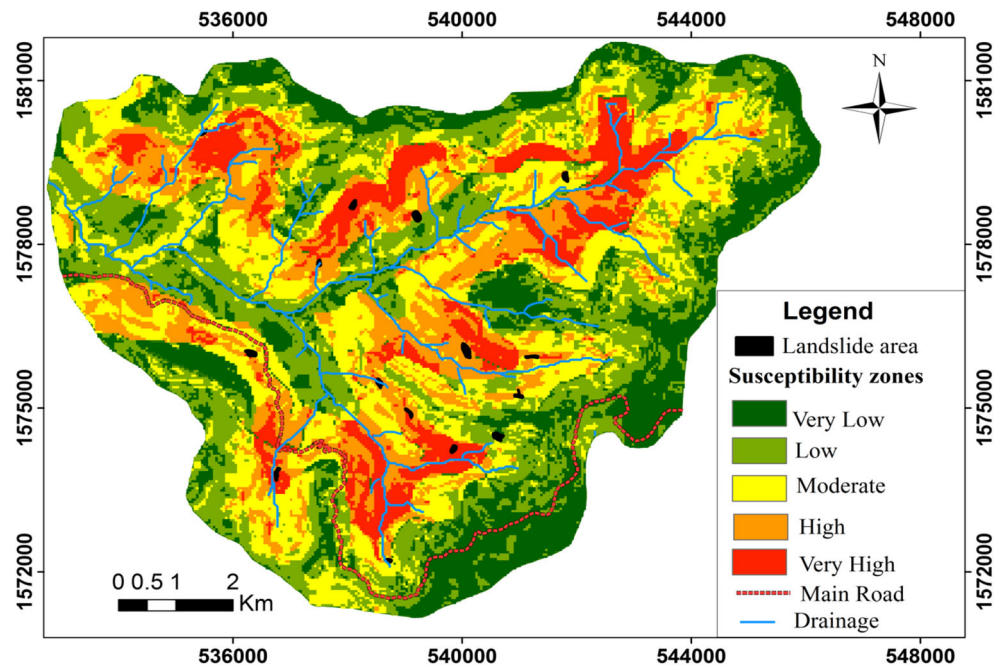

Fig. 14 Cumulative percentage of study area classified as susceptible (*x*-axis) in cumulative percent of landslide occurrence (*y*-axis)
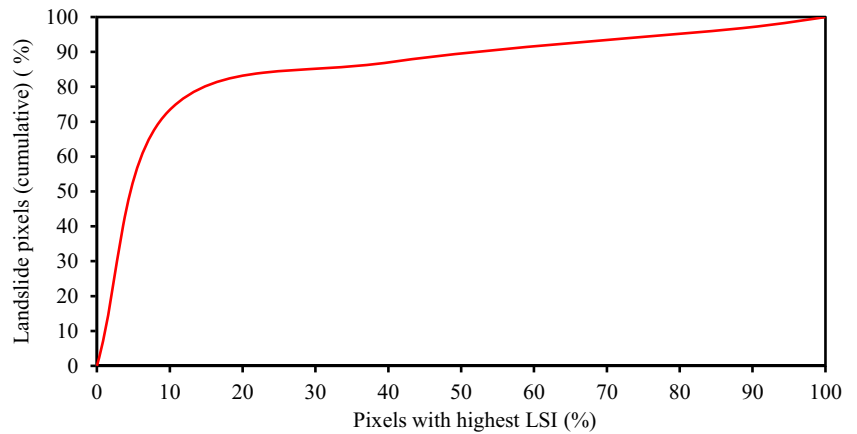
Table 4 Field data for the rock discontinuities and slope characteristics of the selected rock slopes

Lithologic unit	Discontinuity characteristics				Rock slope characteristics			
	Code	Strike/dip	Direction	Internal friction angle	Slope angle	Strike	Direction	Slope height (m)
Basalt (R1)	J1	320°/85°	NE	41°	86°	195°	SE	105
	J2	040°/80°	NW					
	J3	082°/84°	NW					
Red sandstone (R2)	J1	340°/86°	NE	39°	88°	275°	SW	80
	J2	030°/83°	SE					
	J3	105°/80°	SW					
White sandstone (R3)	J1	315°/86°	SW	58°	85°	265°	SE	7
	J2	045°/82°	NW					

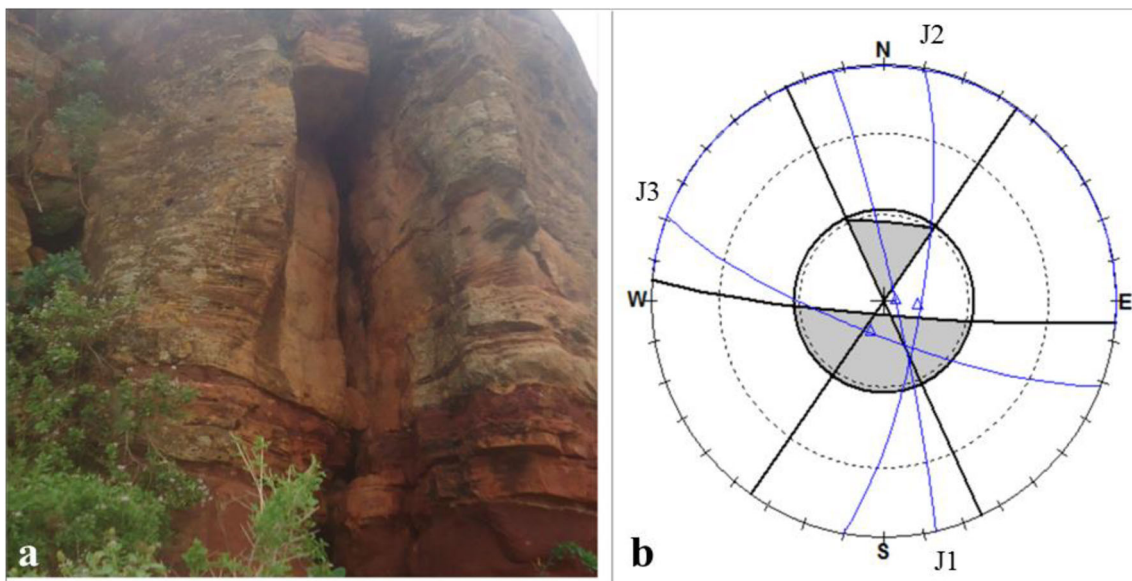For locations, see Fig. 7 (R1, R2, and R3)
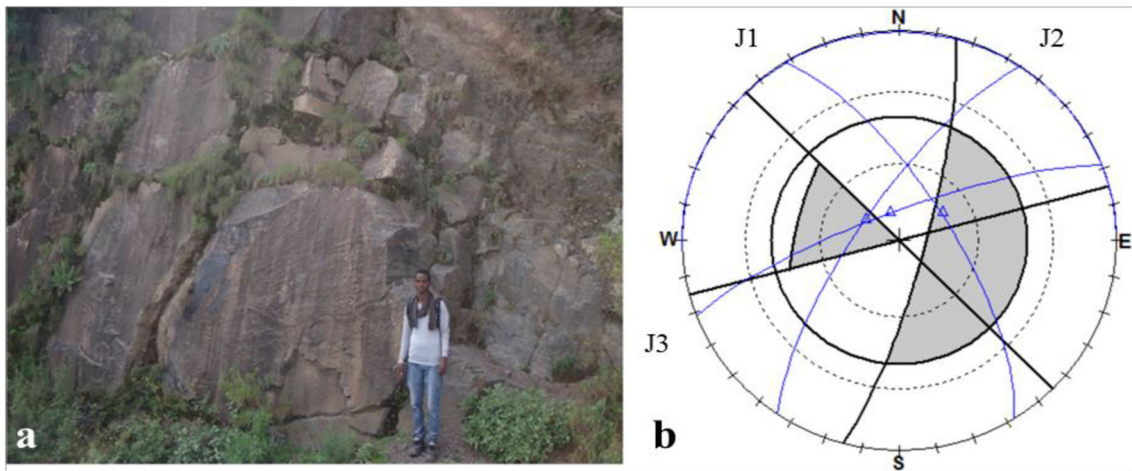
Fig. 15 **a** Outcrop view of rock slope failure surface in basalts. **b** Stereoplots of three discontinuities. Field photograph was taken by the first author on the 13th of August 2018

The white sandstone is characterized by widely spaced vertical joints and moderate degree of weathering, and it is generally massive with rare occurrence of landslides. From the kinematic analysis, potentially topple and marginally planar types of failures were identified (Fig. 17). Field observation confirmed the presence of potentially unstable blocks of rocks at the selected rock slopes.

Conclusion and recommendation

Landslide susceptibility assessment and mapping is crucial for sustainable land-use planning and risk reduction in landslide-prone regions. The factors influencing landslide occurrence

are many, very complex, and many times act simultaneously. Lithology (red sandstone and tillite), distance to stream (0 to 300 m), LULC (bare land and settlement), and slope steepness (> 25°) resulted in FR > 1, indicating strong relationship with landslide occurrence. It was determined that 19.53 and 24.15% of the study area corresponds to very high and high landslide susceptibility zones in the LSM generated with FR, respectively. Low and moderate susceptible zones make up 22.57 and 18.74% of the total area, respectively. The very low susceptible zone value is 15.01%. Based on the different validation approaches, the FR method was found to be suitable for landslide susceptibility mapping for the area and may be applied to other areas with similar topographic and geological settings. Selected rock slope stability analysis using kinematic

Fig. 16 **a** Outcrop view of the rock slope failure in red sandstone and (b) stereoplots of three discontinuities. Field photograph was taken by the second author on the 9th of August 2018
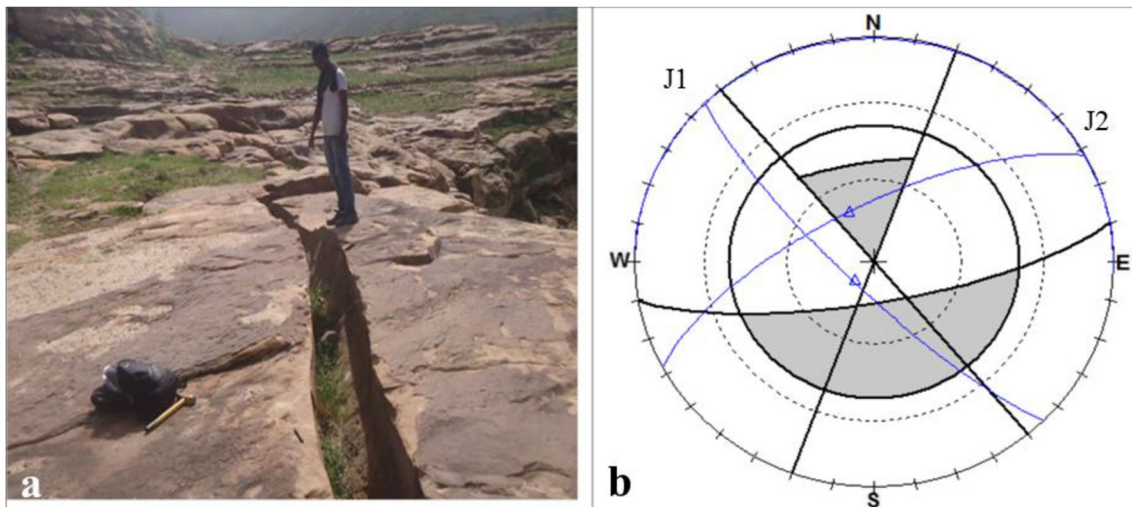
Fig. 17 **a** Outcrop view of rock slope failure in white sandstone and **b** stereoplots of two discontinuities. Field photograph was taken by the second author on the 3rd of August 2018

approach resulted in potential and marginal failures of planar, wedge, and topple types. From the landslide distribution map, rock fall is the predominant (42% of 220 landslides) type of failure.

LSM is an appropriate mean for the evaluation of the degree of landslide susceptibility of an area before administrative and engineering measures are taken. Areas with high and very high landslide susceptibility should be given priority for solutions and need proper land-use planning. Based on the LSM, the high and very high susceptibility zones with high population density and fertile land should be given emphasis in order to reduce future losses and damages. To implement remedial measures, detailed and site-specific multidisciplinary investigations are recommended for hazard and risk estimations.

Compliance with ethical standards

Conflict of interest   The authors declare that they have no conflict of interest.

References

Abebe B, Dramis F, Fubelli G et al (2010) Landslide in Ethiopia highlands and rift margins. J Afr Earth Sci 56:131–138. https://doi.org/10.1016/j.jafrearsci.2009.06.006

AGU (2017) The human cost of landslide in 2016, the landslide blog. American Geophysical Union (AGU) http://blogs.agu.org/landslideblog/

Akgun A, Dag S, Bulut F (2008) Landslide susceptibility mapping for a landslide prone area (Findikli, NE of Turkey) by likelihood frequency ratio and weighted linear combination models. Environ Geol 54:1127–1143

Avinash KG, Ashamanjari KG (2010) A GIS and frequency ratio based landslide susceptibility mapping: Aghnashini river catchment, Uttara Kannada, India. Int J Geomatics Geosci 1(3):343–354

Ayenew T, Barbieri G (2005) Inventory of landslides and susceptibility mapping in the Dessie area, northern Ethiopia. Eng Geol 77:1–15. https://doi.org/10.1016/j.enggeo.2004.07.002

Baharuddin I, Omar R, Roslan R, et al. (2016) Determination of slope instability using spatially integrated mapping framework. In: International Engineering Research and Innovation Symposium (IRIS)

Broothaerts N, Kissi E, Poesen J et al (2012) Spatial patterns, causes and consequences of landslides in the Gilgel gibe catchment, SW Ethiopia. Catena 97:127–136. https://doi.org/10.1016/j.catena.2012.05.011

Chalkias C, Ferentinou M, Polykretis C (2014) GIS-based landslide susceptibility mapping on the Peloponnese Peninsula. Greece Geosci 4:176–190. https://doi.org/10.3390/geosciences4030176

Corominas J, van Westen C, Frattini P, Cascini L, Malet JP, Fotopoulou S, Catani F, Van Den Eeckhaut M, Mavrouli O, Agliardi F, Pitilakis K, Winter MG, Pastor M, Ferlisi S, Tofani V, Hervas J, Smith JT (2014) Recommendations for the quantitative analysis of landslide risk. Bull. Eng. Geol. Environ. 73: 209–263. https://doi.org/10.1007/s10064-013-0538-8

Crozier MJ (2005) Multiple occurrence regional landslide events in New Zealand: hazard management issues. Landslides 2:247–256

Cruden DM (1991) A simple definition of a landslide. Bull Int Assoc Eng Geol 43(1):27–29 https://link.springer.com/article/10.1007%2FBF02590167 ?LI=true

Debarbieux B, Rudaz G (2015) The mountain: a political history from the enlightenment to the present. University of Chicago Press, Chicago

Demir G, Aytekin A, İkizler SB et al (2013) A comparison of landslide susceptibility mapping of the eastern part of the North Anatolian Fault Zone (Turkey) by likelihood-frequency ratio and analytic hierarchy process methods. Nat Hazards 65(3):1481–1506. https://doi.org/10.1007/s11069-012-0418-8

Donati L, Turrini MC (2002) An objective method to rank the importance of the factors predisposing to landslides with the GIS methodology: application to an area of the Apennines (Valnerina, Perugia, Italy). Eng Geol 63:277–289

EMA (1997) Adigrat (1439C2) and Nebelet (1439C4) topographic maps (1:50,000). Ethiopian Mapping Agency, Addis Ababa

Environmental Systems Research Institute (ESRI) (2010) ArcMap10. USA

Ercanoglu M, Gokceoglu C (2004) Use of fuzzy relations to produce landslide susceptibility map of a landslide prone area (West Black Sea region, Turkey). Eng Geol 75:229–250

Frattini P, Crosta G, Carrara A (2010) Techniques for evaluating the performance of landslide susceptibility models. Eng Geol 111(1): 62–72. https://doi.org/10.1016/j.enggeo.2009.12.004

Garland CR (1980) Geology of the Adigrat area. Ministry of Mines, Energy and Water Resources, Geological Survey of Ethiopia, Addis Ababa, Memoir No. 1, 51 pp.

Guzzetti F, Salvati P, Stark C P (2005) Evaluation of risk to the population posed by natural hazards in Italy. In: Landslide risk management. edited by: Hungr, O., Fell, R., Couture, R., and Eberhardt, E., Taylor & Francis Group, London, 381–389

Haque U, da Silva PF, Devoli G, Pilz J, Zhao B, Khaloua A, Wilopo W, Andersen P, Lu P, Lee J, Yamamoto T, Keellings D, Wu JH, Glass GE (2019) The human cost of global warming: deadly landslides and their triggers (1995–2014). Sci Total Environ. https://doi.org/10.1016/j.scitotenv.2019.03.415

Highland L, Bobrowsky P (2008) The landslide handbook- a guide to understanding landslides. U.S. Geological Survey, Reston, Virginia, 147 pp. https://doi.org/10.14358/PERS.70.5.617

Hong H, Chen W, Xu C, Youssef AM, Pradhan B, Bui DT (2016) Rainfall-induced landslide susceptibility assessment at the Chongren area (China) using frequency ratio, certainty factor, and index of entropy. Geocarto Int. https://doi.org/10.1080/10106049.2015.1130086

Hungr O, Leroueil S, Picarelli L (2013) The Varnes classification of landslide types, an update. Landslides. https://doi.org/10.1007/s10346-013-0436-y

Kanungo D, Arora M, Sarkar S et al (2009) Landslide susceptibility zonation (LSZ) mapping – a review. J South Asia Disaster Stud 2: 1–81

Khan H, Shafique M, Khan MA, Bacha MA, Shah SU, Calligaris C (2019) Landslide susceptibility assessment using frequency ratio, a case study of northern Pakistan. The Egypt J Remote Sens Space Sci 22:11–24. https://doi.org/10.1016/j.ejrs.2018.03.004

Lee S, Choi U (2003) Development of GIS based geological hazard information system and its application for landslide analysis in Korea. Geosci J 7:243–252

Lee S, Talib JA (2005) Probabilistic landslide susceptibility and factor effect analysis. Environ Geol 47:982–990

Lee S, Chwae U, Min K (2002) Landslide susceptibility mapping by correlation between topography and geological structure: the Janghung area, Korea. Geomorphology 46:49–162

Luzi L, Pergalani F, Terlien MTJ (2000) Slope vulnerability to earthquakes at sub-regional scale, using probabilistic techniques and geographic information systems. Eng Geol 58:313–336

Mengesha T, Tadiwos C, Workineh H (1996) The geological map of Ethiopia, 1: 2,000,000 scale, 2nd edn. EIGS, Addis Ababa

Mohan R, Jeyaseelan A, Naveen T et al (2011) Landslide susceptibility mapping using frequency ratio method and GIS in south eastern part of Nilgiri District, Tamilnadu, India. J Geo Geosci 1(4):951–961

Nicu IC (2018) Application of analytic hierarchy process, frequency ratio, and statistical index to landslide susceptibility: an approach to endangered cultural heritage. Environ Earth Sci 77:79. https://doi.org/10.1007/s12665-018-7261-5

Pourghasemi HR, Rahmatib O (2018) Prediction of the landslide susceptibility: which algorithm, which precision? Catena 162:177–192. https://doi.org/10.1016/j.catena.2017.11.022

Pourghasemi HR, Goli Jirandeh A, Pradhan B, Xu C, Gokceoglu C (2013) Landslide susceptibility mapping using support vector machine and GIS at the Golestan Province. Iran J Earth Syst Sci 122(2): 349–369

Pourghasemi HR, Yansari ZT, Panagos P, Pradhan B (2018) Analysis and evaluation of landslide susceptibility: a review on articles published during 2005–2016 (periods of 2005–2012 and 2013–2016). Arab J Geosci 11:193. https://doi.org/10.1007/s12517-018-3531-5

Pradhan B, Lee S (2009) Delineation of landslide hazard areas on Penang Island, Malaysia, by using frequency ratio, logistic regression, and artificial neural network model. Environ Earth Sci. https://doi.org/10.1007/s1266500902458

Pradhan B, Lee S (2010) Landslide susceptibility assessment and factor effect analysis: backpropagation artificial neural networks and their comparison with frequency ratio and bivariate logistic regression modelling. Environ Model Softw 25(6):747–759

Pradhan B, Abokharima MH, Jebur MN, Tehrany MS (2014) Land subsidence susceptibility mapping at Kinta Valley (Malaysia) using the evidential belief function model in GIS. Nat Hazards 73:10191042

Price MF, Arnesen T, Gløersen E et al (2019) Mapping mountain areas: learning from global, European and Norwegian perspectives. J Mt Sci 16(1). https://doi.org/10.1007/s11629-018-4916-3

Reichenbach P, Rossi M, Malamud BD, Mihir M, Guzzetti F (2018) A review of statistically-based landslide susceptibility models. Earth Sci Rev 180:60–91. https://doi.org/10.1016/j.earscirev.2018.03.001

Rockware (2003) User's manual: Rockpack III for windows. Rockware, Inc. USA

Saadatkhah N, Kassim A, Lee LM (2014) Qualitative and quantitative landslide susceptibility assessments in Hulu Kelang area, Malaysia. Electron J Geotech Eng 19:545–563

Sarkar S, Kanungo DP (2004) An integrated approach for landslide susceptibility mapping using remote sensing and GIS. Photogramm Eng Remote Sens 70(5):617–625

Sembroni A, Molin P, Dramis F et al (2017) Geology of the Tekeze River basin (Northern Ethiopia). J Maps 13(2):621–631. https://doi.org/10.1080/17445647.2017.1351907

Sun X, Chen J, Bao Y, Han X, Zhan J, Peng W (2018) Landslide susceptibility mapping using logistic regression analysis along the Jinsha River and its tributaries close to Derong and Deqin County, southwestern China. Int J Geo-Inf 7:438. https://doi.org/10.3390/ijgi7110438

Tseng CM, Lin CW, Hsieh WD (2015) Landslide susceptibility analysis by means of event-based multi-temporal landslide inventories. Nat Hazard Earth Syst 3(2):1137–1173

United Nations (2016) Sustainable mountain development. Resolution adopted by the General Assembly on 21 December 2016. Document a/RES/71/234. New York: United Nations

Varnes DJ (1978) Slope movement types and processes. In: Schuster RL, Krizek RJ (eds) Landslides, analysis and control, special report 176: transportation research board. National Academy of Sciences, Washington, DC, pp 11–33

Varnes DJ (1984) International Association of Engineering Geology Commission on Landslides and Other Mass Movements on Slopes: landslide hazard zonation: a review of principles and practice. UNESCO, Paris 63 pp

Vijith H, Madhu G (2007) Estimating potential landslide sites of an upland subwatershed in Western Ghat's of Kerala (India) through frequency ratio and GIS. Environ Geol. https://doi.org/10.1007/s0025400710902

Wieczorek GF (1984) Preparing a detailed landslide-inventory map for hazard evaluation and reduction. Bull Assoc Eng Geol 21(3):337–342

Woldearegay K (2013) Review of the occurrences and influencing factors of landslides in the highlands of Ethiopia: with implications for infrastructural development. Momona Ethiopian J Sci 5:3–31

Wyllie D (2015) Rock fall engineering. Taylor and Francis Group, LLC, Boca Raton

Yalcin A, Reis S, Aydinoglu C et al (2011) A GIS-based comparative study of frequency ratio, analytical hierarchy process, bivariate statistics and logistics regression methods for landslide susceptibility mapping in Trabzon, NE Turkey. Catena 85:274–287. https://doi.org/10.1016/j.catena.2011.01.014

Yan G, Liang S, Gui X, Xie Y, Zhao H (2018) Optimizing landslide susceptibility mapping in the Kongtong District, NW China: comparing the subdivision criteria of factors. Geocarto Int. https://doi.org/10.1080/10106049.2018.1499816

Zezere JL, Reis E, Garcia R et al (2004) Integration of spatial and temporal data for the definition of different landslide hazard scenarios in the area north of Lisbon (Portugal). Nat Hazard Earth Syst Sci 4: 133–146

Zhou C, Yin K, Cao Y et al (2018) Landslide susceptibility modeling applying machine learning methods: a case study from Longju in the Three Gorges Reservoir area, China. Comput Geosci 112:23–37. https://doi.org/10.1016/j.cageo.2017.11.019